Environmental Science & Technology

Article

Cite This: Environ. Sci. Technol. 2019, 53, 11142−11152

pubs.acs.org/est

Reactive Nitrogen Species Are Also Involved in the Transformation of Micropollutants by the UV/Monochloramine Process

Zihao Wu,[†,∥] Chunyan Chen,[†,∥] Ben-Zhan Zhu,[‡] Chun-Hua Huang,[‡] Taicheng An,[§] Fangang Meng,[†] and Jingyun Fang*,[†]

[†]Guangdong Provincial Key Laboratory of Environmental Pollution Control and Remediation Technology, School of Environmental Science and Engineering, Sun Yat-Sen University, Guangzhou 510275, China

[‡]State Key Laboratory of Environmental Chemistry and Ecotoxicology, Research Center for Eco-Environmental Sciences and University of Chinese Academy of Sciences, Chinese Academy of Sciences, Beijing 100085, P. R. China

[§]Guangdong Key Laboratory of Environmental Catalysis and Health Risk Control, School of Environmental Science and Engineering, Institute of Environmental Health and Pollution Control, Guangdong University of Technology, Guangzhou 510006, China

Supporting Information

ABSTRACT: The UV/monochloramine (NH_2Cl) process is an emerging advanced oxidation process (AOP) in water treatment via radicals produced from the UV photolysis of NH_2Cl. This study investigated the degradation of micropollutants by the UV/NH_2Cl AOP, with ibuprofen (IBP) and naproxen (NPX) selected as representative micropollutants. Hydroxyl radical ($HO^•$) and chlorine atom ($Cl^•$) were identified in the process, and unexpectedly, we found that reactive nitrogen species (RNS) also played important roles in the transformation of micropollutants. The electron paramagnetic resonance (EPR) analysis proved the production of $^•NO$ as well as $HO^•$. The concentrations of $HO^•$, $Cl^•$, and $^•NO$ in UV/NH_2Cl remained constant at pH 6.0−8.6, resulting in the slightly changed UV fluence-based pseudo-first-order rate constants (k') of IBP and NPX, which were about 1.65×10^{-3} and 2.54×10^{-3} cm^2/mJ, respectively. For IBP, the relative contribution of RNS to k' was 27.8% at pH 7 and 50 μM NH_2Cl, which was higher than that of $Cl^•$ (6.5%) but lower than that of $HO^•$ (58.7%). For NPX, the relative contribution of RNS to k' was 13.6%, which was lower than both $Cl^•$ (23.2%) and $HO^•$ (46.9%). The concentrations of $HO^•$, $Cl^•$, and $^•NO$ increased with the increasing NH_2Cl dosage. Water matrix components of natural organic matter (NOM) and bicarbonate can scavenge $HO^•$, $Cl^•$, and RNS. The presence of 5 mg/L NOM decreased the k' of IBP and NPX by 66.9 and 57.6%, respectively, while 2 mM bicarbonate decreased the k' of IBP by 57.4% but increased the k' of NPX by 10.5% due to the contribution of $CO_3^{•-}$ to NPX degradation. Products containing nitroso-, hydroxyl-, and chlorine-groups were detected during the degradation of IBP and NPX by UV/NH_2Cl, indicating the role of nitrogen oxide radical ($^•NO$) as well as $HO^•$ and $Cl^•$. Trichloronitromethane formation was strongly enhanced in the UV/NH_2Cl-treated samples, further indicating the important roles of RNS in this process. This study first demonstrates the involvement of RNS in the transformation of micropollutants in UV/NH_2Cl.

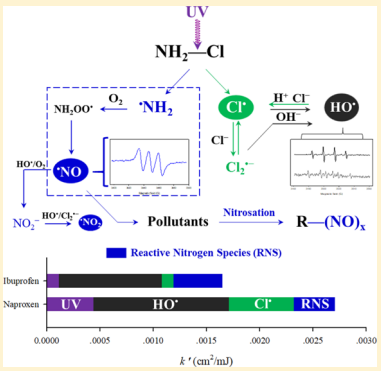

INTRODUCTION

Both free chlorine (Cl_2) and ultraviolet (UV) irradiation are widely used for disinfection of drinking water, swimming pools, and wastewater. The UV/Cl_2 process has been widely investigated as a promising advanced oxidation process (AOP) for the abatement of micropollutants;[1−5] also, it has been applied in a wastewater reuse treatment plant.[6,7] During the UV/Cl_2 treatment of ammonia-containing water, the coexposure of UV and chloramines (UV/chloramine) can occur because ammonia is widely present in aquatic environments and reacts rapidly with chlorine to form chloramines.[8] Additionally, in potable water reuse, permeation of the reverse osmosis (RO) membranes by the chloramines applied upstream results in the de facto UV/chloramine AOP during UV-AOP treatment of the RO permeate.[9] Furthermore, UV treatment of chlorinated swimming pool water induced the UV/chloramine AOP because the concentration of chloramines was around 0.2 mg/L (as Cl_2) in swimming pools.[10,11] All of the above scenarios led to UV/chloramine coexposure in actual water treatment.

The UV photolysis of monochloramine (NH_2Cl) produces a chlorine atom ($Cl^•$) and amidogen radical ($^•NH_2$) (eq 1).[12,13] Although $^•NH_2$ is relatively unreactive, $Cl^•$ can degrade pollutants directly or form secondary radicals such as $HO^•$ and dichlorine radical anion ($Cl_2^{•-}$) (eqs 2−5).[14] The UV/NH_2Cl

Received: February 26, 2019
Revised: August 9, 2019
Accepted: August 14, 2019
Published: August 14, 2019

DOI: 10.1021/acs.est.9b01212
Environ. Sci. Technol. 2019, 53, 11142−11152

AOP is effective for the degradation of micropollutants. It was reported to be effective for the removal of 1,4-dioxane by producing $HO^{\bullet}$ and $Cl_2^{\bullet-}$.[8,15] It was also found to be effective for the degradation of benzoate, carbamazepine, diethyltoluamide, and caffeine by generating $HO^{\bullet}$ and $Cl^{\bullet}$,[15,16] with the contribution of $Cl^{\bullet}$ approaching 50% for benzoate degradation.[15,16] The presence of ammonia enhanced the degradation of metronidazole and diethyltoluamide in UV/Cl_2 treatment by increasing $HO^{\bullet}$ and $Cl^{\bullet}$ production.[4] $HO^{\bullet}$ is important for the removal of micropollutants by the UV/NH_2Cl AOP, while the roles of other radicals such as reactive chlorine species (RCS, i.e., $Cl^{\bullet}$ and $Cl_2^{\bullet-}$) are currently under debate. Based on the experiments using the *tert*-butanol (TBA) radical scavenger, $Cl_2^{\bullet-}$ was reported to be important for the degradation of 1,4-dioxane in the UV/NH_2Cl AOP,[8] whereas the role of $Cl_2^{\bullet-}$ in the degradation of 1,4-dioxane could be neglected according to a kinetic model.[15] The different role of $Cl_2^{\bullet-}$ in the 1,4-dioxane degradation in the two studies probably due to different levels of chloride (Cl^-), as higher Cl^- induced an increase in $Cl_2^{\bullet-}$.[15] Some studies reported that $Cl^{\bullet}$ was not important for the degradation of 1,4-dioxane by UV/NH_2Cl,[8,15,17,18] whereas other studies demonstrated that $Cl^{\bullet}$ was the major reactive species responsible for the degradation of benzoate, diethyltoluamide, and caffeine.[15,16] Thus, the roles of $HO^{\bullet}$ and RCS such as $Cl^{\bullet}$ and $Cl_2^{\bullet-}$ in the degradation of different micropollutants in the UV/NH_2Cl AOP require further investigation.

$$NH_2Cl + h\nu \rightarrow {}^{\bullet}NH_2 + Cl^{\bullet} \qquad \Phi = 0.1 \sim 0.3 \tag{1}$$

$$Cl^{\bullet} + H_2O \rightarrow ClOH^{\bullet-} + H^+ \qquad k = 4.5 \times 10^3\ M^{-1}\ s^{-1} \tag{2}$$

$$Cl^{\bullet} + OH^- \rightarrow ClOH^{\bullet-} \qquad k = 1.8 \times 10^{10}\ M^{-1}\ s^{-1} \tag{3}$$

$$ClOH^{\bullet-} \rightarrow HO^{\bullet} + Cl^- \qquad k = 6.1 \times 10^9\ s^{-1} \tag{4}$$

$$Cl^{\bullet} + Cl^- \leftrightarrow Cl_2^{\bullet-} \qquad k_+ = 6.5 \times 10^9\ M^{-1}\ s^{-1}/k_- = 1.1 \times 10^5\ s^{-1} \tag{5}$$

Reactive nitrogen species (RNS) have not been previously identified in the UV/NH_2Cl AOP. It was reported that nitrate and nitrite were formed in the UV/NH_2Cl system[17,18] and during the coexposure of UV and other chloramines such as $NHCl_2$ or NCl_3.[12,17−19] RNS such as nitrogen dioxide radical (${}^{\bullet}NO_2$) and nitrogen oxide radical (${}^{\bullet}NO$) can be formed as primary radicals by the UV photolysis of nitrate/nitrite (eq 6)[20,21] or can be generated as secondary radicals from the reaction of $HO^{\bullet}$ or $Cl_2^{\bullet-}$ with nitrite (eqs 7 and 8).[22] RNS, particularly ${}^{\bullet}NO$, are common in the atmosphere due to the combustion of waste, coal, and fuel oil,[23] and ${}^{\bullet}NO$ was reported to be effective against some antibiotic-resistant bacteria.[24] RNS were reported to be effective for the removal of many micropollutants such as bisphenol A, estrone, 17α-ethynylestradiol, triclosan, and diclofenac in the coexposure of UV and nitrate.[25] Also, RNS produced by nitrite sunlight photolysis reacted with sulfamethoxazole, emtricitabine, propranolol, trimethoprim, and lamivudine in the wastewater effluent.[26] In the UV/NH_2Cl AOP, RNS probably play roles in the degradation of micropollutants.

$$NO_3^-/NO_2^- + h\nu \rightarrow {}^{\bullet}NO_2/{}^{\bullet}NO + O^{\bullet-} \tag{6}$$

$$HO^{\bullet} + NO_2^- \rightarrow OH^- + {}^{\bullet}NO_2 \qquad k = 0.6 \sim 1.4 \times 10^{10}\ M^{-1}\ s^{-1} \tag{7}$$

$$Cl_2^{\bullet-} + NO_2^- \rightarrow 2Cl^- + {}^{\bullet}NO_2 \qquad k = 2.5 \times 10^8\ M^{-1}\ s^{-1} \tag{8}$$

Transformation pathways during the abatement of micropollutants by oxidation processes are important for the evaluation of a specific process. RCS were reported to produce chloroproducts.[1,2,5,27,28] For RNS, nitro-group addition was reported on the ortho/para position of phenolic compounds by ${}^{\bullet}NO_2$ oxidation.[29,30] For disinfection byproducts (DBPs), chloroform (TCM) was reported to be the dominant DBP in the degradation of diethyltoluamide and caffeine by UV/NH_2Cl, whereas nitrogenous DBPs (N-DBPs) such as trichloroacetonitrile and dichloroacetonitrile (DCAN) were not observed.[16] On the other hand, N-DBPs such as N-nitrosamines,[13] chloropicrin (TCNM),[31] and DCAN[11] were reported to form at higher contents under UV/chloramine coexposure scenarios than under chloramination alone. Thus, the transformation pathways and DBP formation during the degradation of micropollutants by UV/NH_2Cl treatment require further investigation.

Therefore, the objectives of this study were to investigate the roles of radicals such as $HO^{\bullet}$, RCS, and RNS in the degradation kinetics and pathways of micropollutants by UV/NH_2Cl treatment. Electron paramagnetic resonance (EPR) technique was used to illustrate the production of RNS and $HO^{\bullet}$. Ibuprofen (IBP) and naproxen (NPX) (Table S1) were selected as the representative micropollutants due to their different reactivities with RCS as reported in our previous study.[3]

MATERIALS AND METHODS

Materials. All solutions were prepared with reagent-grade chemicals and purified water (18.2 MΩ cm) produced from a Milli-Q system (Millipore, Reference). IBP (98%), NPX (98%), nitrobenzene (NB) (99%), benzoic acid (BA), 1,4-dimethoxybenzene (DMOB), hydrogen peroxide (H_2O_2) solution (available H_2O_2 30%), sodium hypochlorite (NaOCl) solution (available chlorine, 4.00−4.99%), and 5,5-dimethyl-1-pyrroline *N*-oxide (DMPO) were purchased from Sigma-Aldrich (St. Louis, MO, USA). TBA was purchased from Alfa Aesar. Suwannee River natural organic matter (NOM) (cat. no. 2R101N) was obtained from the International Humic Substances Society. High-performance liquid chromatography (HPLC) grade methanol, acetonitrile, *o*-phosphoric acid, and dimethylsulfoxide (DMSO) were obtained from Fisher Scientific. Sodium bicarbonate ($NaHCO_3$) and ammonium chloride (NH_4Cl), ferrous sulfate ($FeSO_4$), sodium hyposulfite ($Na_2S_2O_4$), and diethyldithiocarbamate (DETC) were purchased from Sinopharm Chemical Reagent Co., Ltd. (Shanghai, China). A fresh NH_2Cl solution was prepared daily by adding NaOCl solution to NH_4Cl solution at a chlorine to ammonia-N mass ratio of 4:1 under rapid stirring for over 40 min.[32]

Experimental Procedures. The photochemical experiments were carried out in a 700 mL, magnetically stirred, cylindrical borosilicate glass reactor with a quartz sleeve in the center in which a low-pressure mercury lamp (Heraeus GPH

DOI: 10.1021/acs.est.9b01212
Environ. Sci. Technol. 2019, 53, 11142−11152

212T5L/4, 10 W) was placed. The UV lamp was turned on at least 30 min prior to the experiments in order to warm up. All experiments were conducted at a temperature of 25 ± 0.2 °C maintained by a water circulating system. The UV photon flux (I_0) entering the solution was determined to be 0.471 μE s^{-1} by iodide/iodate chemical actinometry.[33] The effective path length (L) was determined to be 2.43 cm by measuring the photolysis kinetics of dilute H_2O_2 (Figure S1).[34] The corresponding average UV fluence rate (E_p^0) was approximately 0.77 mW cm^{-2}.

A test solution (700 mL) at pH 7 (2 mM phosphate buffer) containing 5 μM IBP or NPX was exposed to UV irradiation and dosed with 50 μM NH_2Cl at the same time. The samples were collected at different time intervals and quenched with ascorbic acid. The effects of NH_2Cl dosages (10, 20, and 50 μM), pH (6.0, 7.0 and 8.6), NOM concentrations (1 and 5 mg/L), and alkalinity (1 and 2 mM HCO_3^-) were investigated. Control tests of IBP and NPX degradation by NH_2Cl alone or direct UV photolysis were conducted in a similar manner but in the absence of UV light or NH_2Cl, respectively. All of the tests were conducted at least twice. The error bars in all the plots of the obtained data represent the maximum and minimum of the experimental data of the duplicated test results.

To identify the products and DBP formation during IBP and NPX degradation by the UV/NH_2Cl AOP, higher initial concentrations of IBP (50 μM), NPX (50 μM), and NH_2Cl (500 μM) were used. After a certain reaction time, the reaction was quenched with ascorbic acid. Then, a 500 mL sample was concentrated to 2 mL by solid-phase extraction using a HLB cartridge (200 mg, 6 mL, Waters) according to the procedure described in the literature,[35] for ultra-HPLC-quadrupole-time of flight-mass spectrometry (UPLC-Q-TOF-MS) (Waters Synapt G2-Si, USA) analysis. Another 20 mL of sample was subjected to liquid−liquid extraction for gas chromatography (Agilent 7890B) analysis. The sample pretreatment details are shown in Text S1.

Analytical Methods. The concentrations of IBP, NPX, NB, BA, and DMOB were quantified by the HPLC system equipped with a C18 column (Poroshell, 4.6 × 50 mm, 2.7 μm) following the method in the literature studies.[36,37] The concentrations of chlorine and NH_2Cl were determined using the DPD/FAS titration method.[38] The pH was measured using a pH meter (FE20, Mettler Toledo). The second-order rate constants of $Cl^\bullet$ reacting with IBP and NPX were determined using a LKS80 laser flash photolysis system, following the method described in a literature.[39]

The EPR experiments were conducted at room temperature, and the spectra were recorded at a Bruker EMX-plus EPR spectrometer. The $^\bullet$NO spin-trapping agent $(DETC)_2-Fe^{2+}$ was freshly prepared by mixing DETC and $FeSO_4$ at a molar ratio of 2:1.[40] The spin-trapping agent of $(DETC)_2-Fe^{2+}$ or DMPO was mixed with NH_2Cl under UV photolysis at pH 7 for 10 and 3 min, respectively, for the identification of $^\bullet$NO or $HO^\bullet$. Then, the sample solution was transferred into a capillary tube, which was then fixed in the cavity resonator of the EPR spectrometer. An additional test was conducted by spiking both DMPO and DMSO into the NH_2Cl solution under UV photolysis, to further prove the production of $HO^\bullet$.[41,42]

The degradation products of IBP and NPX were identified by UPLC-Q-TOF-MS and equipped with an electrospray interface (ESI). The negative ESI mode was used to identify the products during the degradation of IBP and NPX. The structures of the main products were further ascertained by high-resolution MS and MS^2 spectra, and their isomeric structures were differentiated by UPLC retention times in the total ion chromatogram. A C18 column (Waters acquity BEH, 1.7 μm) was used to separate the products. The details of the chromatographic and mass conditions of UPLC-Q-TOF-MS analysis are described in Text S2.

DBPs including chloroform (TCM), 1,1-dichloro-2-propanone (1,1-DCP), 1,1,1-trichloropropanone (1,1,1-TCP), trichloronitromethane (TCNM), and DCAN were quantified by a gas chromatograph (GC) following the USEPA Method 551.1,[43] and the GC was coupled with an electron capture detector and equipped with an HP-5 fused silica capillary column (30 m × 0.25 mm, 0.25 mm, J&W Scientific, Folsom, CA).

Quantum Chemistry Calculations. All calculations for structural optimizations and molecular orbital distributions were performed based on density functional theory at the B3LYP/6-31G (2df,p) level and integral equation formalism polarizable continuum model (IEFPCM) using the Gaussian 09 program.[44] Structural optimization was conducted without any symmetry constraints, and the minima were verified by vibrational analysis. The molecular orbital distribution contained the highest occupied molecular orbitals (HOMO).

Kinetic Modeling. The concentrations of different reactive species were simulated by kinetic modeling using Kintecus software.[45] The kinetic model included the coupled reactions related to RCS[4,15,28] and additional reactions related to RNS.[12,22,46,47] Details of the reactions are shown in Table S2.

RESULTS AND DISCUSSION

Identification of RNS and $HO^\bullet$ in the UV/NH_2Cl AOP. Figure 1a shows the EPR spectra of $^\bullet$NO trapped by $(DETC)_2-Fe^{2+}$ in UV/NH_2Cl. A control test of a $^\bullet$NO standard sample trapped by $(DETC)_2-Fe^{2+}$ was also conducted, which presented the same EPR signal as that in UV/NH_2Cl (shown in the bottom of Figure 1a). The $(DETC)_2-Fe^{2+}-NO$ spin adduct (eq 9) is characterized by the isotropic EPR signal at g value of 2.035 with a triplet superhyperfine structure (a^N) of 13.5 G.[40] The signal intensity of $^\bullet$NO increased with increasing NH_2Cl dosage, while it was not obvious in the UV/NH_2Cl system saturated by N_2.

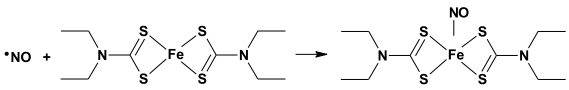

(9)

$^\bullet NH_2$ can rapidly react with O_2 to generate aminylperoxyl radicals ($NH_2OO^\bullet$) at a rate constant of 3.8×10^8 M^{-1} s^{-1} (eq 10),[22] then $NH_2OO^\bullet$ rapidly reacts with H_2O to form $HNOOH-H_2O$ and further decay to $^\bullet$NO at rate constant of 1 to 2 × 10^9 M^{-1} s^{-1} (eq 11).[46,48] The saturation of N_2 decreased >90% dissolved O_2 in the solution; thus, the formation of $^\bullet$NO decreased significantly. Note that nitrite and nitrate were also produced in the UV/NH_2Cl system with the concentration of ∼3 μM at 50 μM NH_2Cl (Figure S2). However, the production of $^\bullet$NO by the UV photolysis of nitrite (eq 6) was negligible because the EPR signal of $^\bullet$NO was undetectable during the photolysis of either 3 μM nitrite or 3 μM nitrate (data not shown).

$$^\bullet NH_2 + O_2 \rightarrow NH_2OO^\bullet \qquad k = 3.8 \times 10^8\ M^{-1}\ s^{-1} \tag{10}$$

DOI: 10.1021/acs.est.9b01212
Environ. Sci. Technol. 2019, 53, 11142−11152

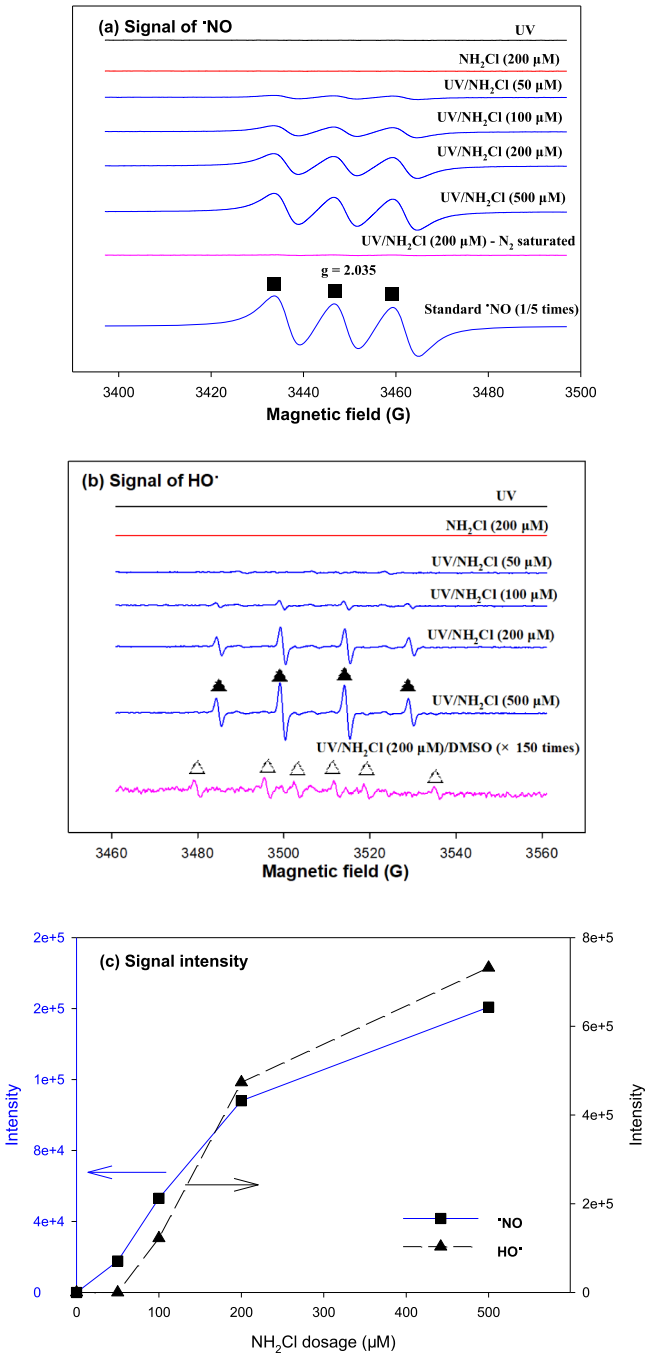

Figure 1. EPR spectra of (a) $^{\bullet}$NO trapped by $(DETC)_2-Fe^{2+}$ and (b) HO$^{\bullet}$ trapped by DMPO, and (c) the EPR spectra intensity of $^{\bullet}$NO (blue line) and HO$^{\bullet}$ (black line) as a function of NH_2Cl dosage in the UV/NH_2Cl system. The EPR spectra of a $^{\bullet}$NO standard sample is shown at the bottom of (a). $(DETC)_2-Fe^{2+}-NO$, ■; DMPO−HO$^{\bullet}$, ▲; DMPO−$CH_3^{\bullet}$, △. Conditions: $[NH_2Cl]_0$ = 50, 100, 200, and 500 μM, $[(DETC)_2-Fe^{2+}]_0$ = 6.7 mM, $[DMPO]_0$ = 0.1 M, $[DMSO]_0$ = 2.8 M.

$$NH_2OO^{\bullet} + H_2O \rightarrow (HNOOH-H_2O) \rightarrow {}^{\bullet}NO + 2H_2O \quad k = 1 \sim 2 \times 10^9\ M^{-1}\ s^{-1} \tag{11}$$

Figure 1b shows typical EPR signals of DMPO−OH in the UV/NH_2Cl system. The signal of DMPO−OH spin adduct has a quartet superhyperfine structure of $a^H = a^N$ = 14.9 G with peak height ratios of 1:2:2:1.[49] It should be noted that a similar DMPO−OH signal may arise from the decomposition of DMPO−OOH.[41] An additional test was thus conducted to confirm the production of HO$^{\bullet}$ in the UV/NH_2Cl system. DMSO reacts with HO$^{\bullet}$ to form methyl radicals ($CH_3^{\bullet}$) (eq 12), which can be trapped by DMPO to yield a corresponding DMPO−CH_3 (eq 13) spin adduct with a sextet superhyperfine structure of a^H = 19.3 G and a^N = 16.4 G.[41] The signal of DMPO−OH and DMPO−CH_3 proved the existence of HO$^{\bullet}$ in the UV/NH_2Cl system.

$$HO^{\bullet} + (CH_3)_2SO \rightarrow CH_3SO_2H + CH_3^{\bullet} \tag{12}$$

$$CH_3^{\bullet} + DMPO \rightarrow DMPO-CH_3 \tag{13}$$

The EPR signals of both $^{\bullet}$NO and HO$^{\bullet}$ increased with the increasing NH_2Cl dosage (Figure 1c). The increases were more rapid at lower NH_2Cl dosage (<200 μM), as excess NH_2Cl scavenged radicals such as $^{\bullet}NH_2$, Cl$^{\bullet}$, and HO$^{\bullet}$ (eqs 113, 111, and 110 in Table S2).

Quantification of Radicals. By using a kinetic modeling, the concentrations of HO$^{\bullet}$ and Cl$^{\bullet}$ were calculated to be $\sim 10^{-13}$ and $\sim 10^{-14}$ M, respectively, whereas those of RNS such as $^{\bullet}$NO and $^{\bullet}NO_2$ were calculated to be $\sim 10^{-9}$ and $\sim 10^{-12}$ M, respectively, in UV/NH_2Cl (Table 1). To validate the kinetic modeling, the concentrations of HO$^{\bullet}$, Cl$^{\bullet}$, and ClO$^{\bullet}$ were determined by using radical probes of NB, BA, and DMOB, following the method described in Hua et al.,[37] with details shown in Text S4. The concentrations of HO$^{\bullet}$, Cl$^{\bullet}$ obtained from the experiment were in good agreement with the model (Table 1 and Figure S3); meanwhile, the concentration of ClO$^{\bullet}$ was negligible from the results of experiment and modeling. The steady-state concentrations of HO$^{\bullet}$, Cl$^{\bullet}$, and $^{\bullet}$NO kept almost constant at pH 6.0−8.6 (Table 1), mainly due to that the photolysis rate of NH_2Cl was pH-independent (Figure S4).

Therefore, based on the confirmation of the radicals existed in the UV/NH_2Cl system, the primary reactions of radical transformation are summarized in Scheme 1. The photolysis of NH_2Cl produced Cl$^{\bullet}$ and $^{\bullet}NH_2$ (eq 1),[12,13] and then, Cl$^{\bullet}$ formed secondary radicals such as HO$^{\bullet}$ and $Cl_2^{\bullet-}$ (eqs 2−5).[14] $^{\bullet}NH_2$ reacts rapidly with O_2 to generate $NH_2OO^{\bullet}$,[22] which then transformed into $^{\bullet}$NO.[46,48] $^{\bullet}$NO reacts with HO$^{\bullet}$ or O_2 to further form nitrite in the UV/NH_2Cl system,[50] which reacts quickly with HO$^{\bullet}$ or $Cl_2^{\bullet-}$ to produce $^{\bullet}NO_2$ (eqs 7 and 8).[22]

Kinetics and Roles of Reactive Species for the Degradation of IBP and NPX by the UV/NH_2Cl AOP. Figure S5 compares the UV fluence-based pseudo-first-order rate constants (k') of the degradation of IBP and NPX by the UV/NH_2Cl and UV/Cl_2 AOPs in pure water at the same molar oxidant dosages (50 μM) and pH 7. The overall k' of IBP degradation by UV/Cl_2 (1.34×10^{-3} cm^2/mJ) was 18.7% lower than that for the degradation by UV/NH_2Cl (1.65×10^{-3} cm^2/mJ), whereas the overall k' for NPX degradation was 2.1 times higher with UV/Cl_2 (8.50×10^{-3} cm^2/mJ) than with UV/NH_2Cl (2.71×10^{-3} cm^2/mJ).

Based on the radical chemistry of the UV/NH_2Cl system as discussed above, the k' of IBP and NPX by UV/NH_2Cl can be attributable to UV, HO$^{\bullet}$, Cl$^{\bullet}$, $Cl_2^{\bullet-}$, and RNS (eq 14).

$$k' = k'_{UV} + k'_{HO^{\bullet}} + k'_{Cl^{\bullet}} + k'_{Cl_2^{\bullet-}} + k'_{RNS} \tag{14}$$

DOI: 10.1021/acs.est.9b01212
Environ. Sci. Technol. 2019, 53, 11142−11152

Table 1. Simulated Molar Concentrations of HO•, Cl•, $Cl_2^{\bullet-}$, •NO, and •NO_2 and Experimentally Determined Steady-State Concentrations of HO• and Cl• in the UV/NH_2Cl System at Different Conditions

NH_2Cl dosage(μM)	pH	HO• (M)	Cl• (M)	$Cl_2^{\bullet-}$ (M)	•NO (M)	•NO_2 (M)
10	7	2.14×10^{-13}	7.14×10^{-15}	2.09×10^{-14}	2.34×10^{-9}	2.64×10^{-12}
20	7	2.40×10^{-13}	1.34×10^{-14}	7.88×10^{-14}	3.30×10^{-9}	3.93×10^{-12}
50	7	2.50×10^{-13}	2.88×10^{-14}	4.28×10^{-13}	5.09×10^{-9}	9.31×10^{-12}
		2.67×10^{-13}[a]	3.42×10^{-14}[a]			
50	6	2.52×10^{-13}	2.82×10^{-14}	4.13×10^{-13}	5.15×10^{-9}	9.11×10^{-12}
		2.64×10^{-13}[a]	3.38×10^{-14}[a]			
50	8.6	2.51×10^{-13}	2.86×10^{-14}	4.25×10^{-13}	5.08×10^{-9}	6.76×10^{-12}
		2.63×10^{-13}[a]	2.96×10^{-14}[a]			

[a]Represents the experimentally determined steady-state concentrations.

Scheme 1. Primary Reactions During UV Photolysis of NH_2Cl

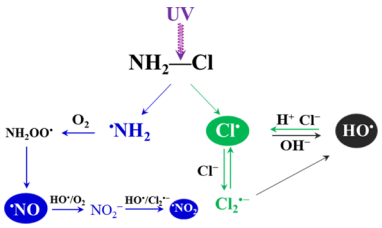

where k'_{UV}, $k'_{HO\bullet}$, $k'_{Cl\bullet}$, $k'_{Cl_2\bullet-}$, and k'_{RNS} are defined as the specific k' by UV direct photolysis, HO•, Cl•, $Cl_2^{\bullet-}$, and RNS, respectively.

To evaluate the roles of the different radicals in the degradation of micropollutants by the UV/NH_2Cl AOP, the radical scavenger of TBA was used (Figure S6). TBA at 50 mM almost completely scavenged HO• ($k = 6 \times 10^8$ M^{-1} s^{-1}) and Cl• ($k = 3 \times 10^8$ M^{-1} s^{-1}), but it has a negligible scavenging effect on $Cl_2^{\bullet-}$ ($k = 700$ M^{-1} s^{-1}).[4,22,51] Therefore, $Cl_2^{\bullet-}$ presents in the UV/NH_2Cl system with 50 mM TBA. The overall k' in the presence of TBA decreased to k'_{UV} for both IBP and NPX, indicating the negligible contribution of $Cl_2^{\bullet-}$ to the IBP and NPX degradation. Thus, the degradation of IBP and NPX by UV/NH_2Cl can be attributable to UV, HO•, Cl•, and RNS, among which k'_{UV} can be obtained by UV direct photolysis tests.

The specific k' of HO•, Cl• in the UV/NH_2Cl AOP depended on the steady-state concentrations of HO• ($[HO^\bullet]_{ss}$) and Cl• ($[Cl^\bullet]_{ss}$) and the second-order rate constants of HO• ($k_{HO\bullet}$) and Cl• ($k_{Cl\bullet}$) (eqs 15 and 16). Then, the specific k' by RNS (k'_{RNS}) can be determined by eq 17.

$$k'_{HO\bullet} = k_{HO\bullet}[HO^\bullet]_{ss} \quad (15)$$

$$k'_{Cl\bullet} = k_{Cl\bullet}[Cl^\bullet]_{ss} \quad (16)$$

$$k'_{RNS} = k' - (k'_{HO\bullet} + k'_{Cl\bullet} + k'_{UV}) \quad (17)$$

The steady-state concentrations of HO• and Cl• were experimentally determined by using NB and BA as the probe compounds, following the method described in Fang et al.[52] (Text S4 and Figure S7). The second-order rate constants for HO• reacting with IBP and NPX were determined to be 5.74×10^9 M^{-1} s^{-1} and 8.16×10^9 M^{-1} s^{-1}, respectively (Figure S8). The second-order rate constants of Cl• reacting with IBP and NPX were determined to be 1.3 ($\pm$0.2) $\times 10^{10}$ and 2.7 ($\pm$0.3) $\times 10^{10}$ M^{-1} s^{-1}, respectively (details shown in Text S3 and Figure S9).

The specific k' of UV, HO•, Cl•, and RNS for the degradation of IBP and NPX in the UV/NH_2Cl AOP at 50 μM NH_2Cl and pH 7 are shown in Figure 2. Specifically, for IBP, the relative contributions of HO•, Cl•, and RNS in UV/NH_2Cl were 58.7, 6.5, and 27.8%, respectively, and those for NPX were 46.9, 23.2, and 13.6%, respectively, indicating that RNS also played important roles in the IBP and NPX degradation. As compared to UV/Cl_2 AOP, the UV/NH_2Cl

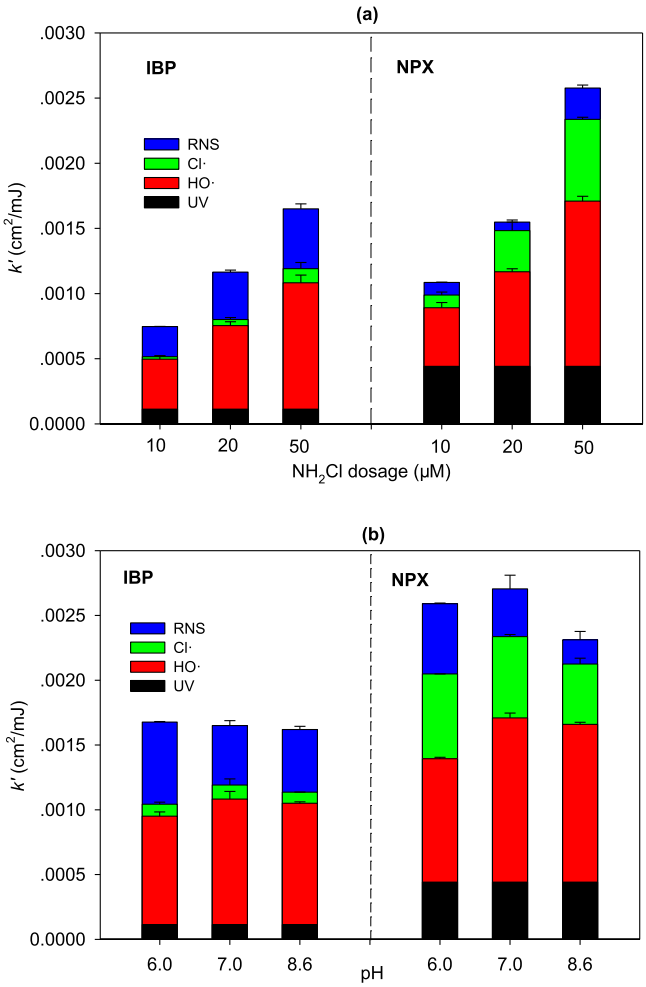

Figure 2. Effects of (a) NH_2Cl dosage and (b) pH on the k' of IBP and NPX and the specific k' by UV, HO•, Cl• and RNS in the UV/NH_2Cl AOP. Conditions: (a) $[IBP]_0 = [NPX]_0 = 5$ μM, $[NB]_0 = [BA]_0 = 1$ μM, pH = 7. (b) $[NH_2Cl]_0 = 50$ μM, $[IBP]_0 = [NPX]_0 = 5$ μM, $[NB]_0 = [BA]_0 = 1$ μM.

DOI: 10.1021/acs.est.9b01212
Environ. Sci. Technol. 2019, 53, 11142−11152

AOP possessed higher $k'_{HO^\bullet}$ for both IBP and NPX and the unique roles of RNS, but the contribution of $ClO^\bullet$ was significant to NPX degradation in UV/Cl_2 (Figure S5). The determination of the specific k' of UV, $HO^\bullet$, $Cl^\bullet$, and other radicals in Figure S5 was similar to that described above, except for the RNS replaced by other radicals.

Effect of NH_2Cl Dosage and pH. Figure 2a shows the k' for IBP and NPX degradation by UV/NH_2Cl at the NH_2Cl dosages of 10, 20, and 50 μM. The k' of IBP and NPX increased with increasing NH_2Cl dosage, while the increasing rate was nonlinear but slowed down gradually, indicating the nonlinear concentrations of the radicals as a function of NH_2Cl dosage. Upon increasing the NH_2Cl dosage from 10 to 20 μM, the k' of IBP and NPX increased by 56.1 and 42.7%, respectively, with increases of 41.7 and 66.4% at NH_2Cl dosage increased from 20 to 50 μM, respectively. Besides, the increase in $k'_{HO^\bullet}$ and $k'_{Cl^\bullet}$ slowed down with the increasing NH_2Cl dosage, mainly due to the scavenging effect on $HO^\bullet$ and $Cl^\bullet$ by NH_2Cl (eqs 18 and 19), which generated $NHCl^\bullet$. $NHCl^\bullet$ can then react with O_2 to form RNS.[8,12] The modeling results show that the concentrations of $HO^\bullet$ and $Cl^\bullet$ increased by 17% and 3 times as the NH_2Cl dosage increased from 10 to 50 μM and that of $^\bullet NO$ increased by 118%. The concentration of $^\bullet NO_2$ was 3 orders of magnitudes lower than that of $^\bullet NO$ (Table 1). Therefore, the increase in the k'_{RNS} was mainly attributed to $^\bullet NO$ rather than $^\bullet NO_2$.

$$NH_2Cl + HO^\bullet \rightarrow NHCl^\bullet + H_2O$$
$$k_{NH_2Cl/HO^\bullet} = 5.1 \times 10^8\ M^{-1}\ s^{-1} \quad (18)$$

$$NH_2Cl + Cl^\bullet \rightarrow NHCl^\bullet + HCl$$
$$k_{NH_2Cl/Cl^\bullet} = 10^8 \sim 10^9\ M^{-1}\ s^{-1} \quad (19)$$

Figure 2b shows the k' for IBP and NPX degradation by the UV/NH_2Cl AOP at different pH levels. For IBP, the overall k' at pH 6.0−8.6 remained constant at 1.62 to 1.68 × 10^{-3} cm^2/mJ. For NPX, the overall k' was 2.31 × 10^{-3} cm^2/mJ at pH 8.6, which was slightly lower than 2.59 to 2.71 × 10^{-3} cm^2/mJ at pH levels of 6.0 and 7.0. The variation of $k'_{HO^\bullet}$ for IBP and NPX was <9%, whereas the $k'_{Cl^\bullet}$ for IBP and NPX decreased by 20.4 and 25.7%, respectively, with increasing pH from 7.0 to 8.6, mainly due to that more $Cl^\bullet$ was consumed by HO^- at higher pH. The modeling results (Table 1) showed a similar trend at different pH values, the concentrations of $HO^\bullet$, $Cl^\bullet$, and $^\bullet NO$ slightly changed, which maintained at 2.50 to 2.52 × 10^{-13}, 2.82 to 2.88 × 10^{-14}, and 5.08 to 5.15 × 10^{-9} M, respectively. The concentrations of radicals remained constant with increasing pH, further suggesting that the effect of pH on UV/NH_2Cl is not important.

Effect of NOM and Alkalinity. NOM retarded the degradation of IBP and NPX in the UV/NH_2Cl AOP, and the decrease in k' for IBP and NPX increased with the increasing NOM concentration (Figure 3a). As the concentration of NOM increased from 0 to 5 mg/L, the k' for IBP decreased from 1.77 × 10^{-3} to 5.85 × 10^{-4} cm^2/mJ and that of NPX decreased from 2.45 × 10^{-3} to 1.04 × 10^{-3} cm^2/mJ. Specifically, $k'_{HO^\bullet}$ decreased by 61.6% and by 62.3% for IBP and NPX, respectively, $k'_{Cl^\bullet}$ decreased by 87.5% and by 64.9% and k'_{RNS} decreased by 78.2% and by 29.7%, respectively. The second-order rate constants for NOM reacting with $HO^\bullet$ and $Cl^\bullet$ were reported to be 2.5 × 10^4 and 1.3 × 10^4 $(mg/L)^{-1}$ s^{-1}, respectively.[52] This indicates that NOM can significantly inhibit the degradation of IBP and NPX by consuming $HO^\bullet$ and $Cl^\bullet$. Additionally, NOM acts as an inner filter with the molar absorption coefficient (ε_{254nm}) of 3.15 $(m^{-1}(mg/L)^{-1})$.[52] In total, 30.4 and 45.7% of UV light was filtered by 5 mg/L NOM in the IBP and NPX solution, respectively. The inner filter reduced the photolysis of NH_2Cl, resulting in lower radical production.

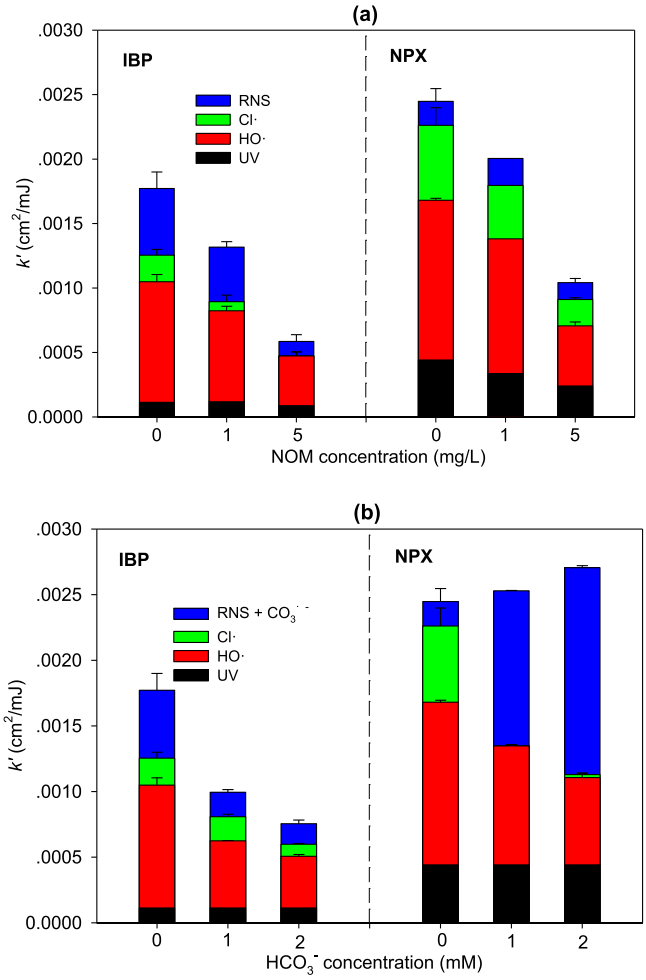

Figure 3. Effects of (a) NOM and (b) bicarbonate on the k' of IBP and NPX and the specific k' by UV, $HO^\bullet$, $Cl^\bullet$ and (a) RNS, (b) RNS + $CO_3^{\bullet-}$ in the UV/NH_2Cl AOP. Conditions: $[NH_2Cl]_0$ = 50 μM, $[IBP]_0$ = $[NPX]_0$ = 5 μM, $[NB]_0$ = $[BA]_0$ = 1 μM, pH = 7.

The presence of HCO_3^- decreased the k' of IBP, and this decrease was enhanced with increasing HCO_3^- concentration. Conversely, the k' of NPX increased with increasing HCO_3^- concentration. When increasing the HCO_3^- concentration from 0 to 2 mM, the k' of IBP decreased by 57.4%, whereas the k' of NPX increased by 10.5% (Figure 3b). $k'_{HO^\bullet}$ values of IBP and NPX decreased by 57.9 and 46.3%, respectively, due to the consumption of $HO^\bullet$ by HCO_3^- (eq 20).[4] Similarly, $k'_{Cl^\bullet}$ of IBP and NPX decreased significantly by 55.5 and 96.1%, respectively, due to the scavenging effect on $Cl^\bullet$ by HCO_3^- (eq 21). However, the formed $CO_3^{\bullet-}$ was reactive with NPX, as the second-order rate constant of $CO_3^{\bullet-}$ reacting with NPX was reported to be 5.6 × 10^7 M^{-1} s^{-1}.[22] Thus, the $k'_{RNS+CO_3^{\bullet-}}$ of NPX increased by 7.5 times, mainly due to the significant contribution of $CO_3^{\bullet-}$ to NPX degradation, which compensated for the decreased contributions of $Cl^\bullet$ and RNS.

DOI: 10.1021/acs.est.9b01212
Environ. Sci. Technol. 2019, 53, 11142−11152

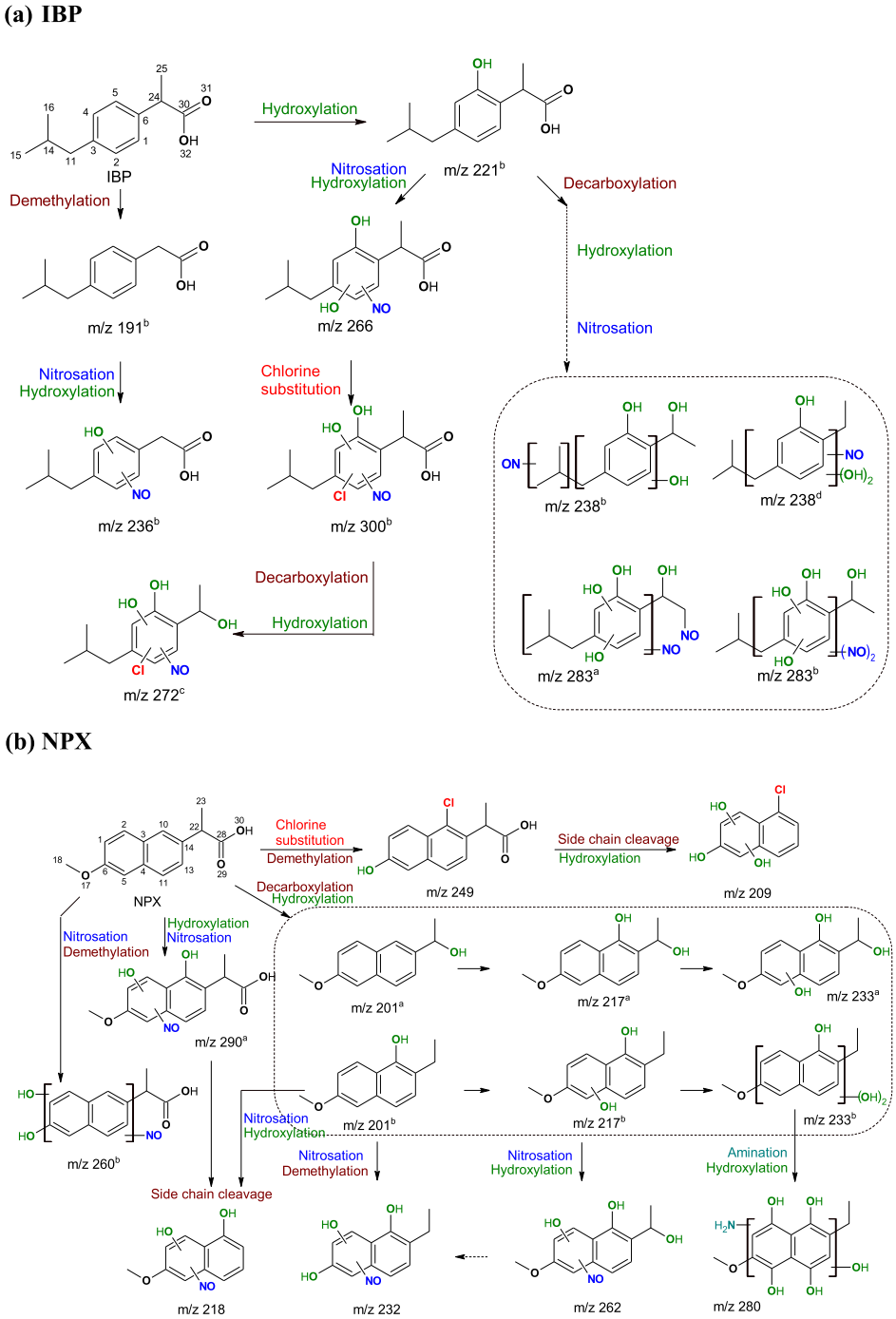

Figure 4. Proposed pathways of the degradation of (a) IBP and (b) NPX by the UV/NH_2Cl AOP.

$$HCO_3^- + HO^\bullet \rightarrow CO_3^{\bullet -} + H_2O$$

$$k_{HCO_3^-/HO^\bullet} = 8.5 \times 10^6\ M^{-1}\ s^{-1} \quad (20)$$

$$HCO_3^- + Cl^\bullet \rightarrow CO_3^{\bullet -} + HCl$$

$$k_{HCO_3^-/Cl^\bullet} = 2.2 \times 10^8\ M^{-1}\ s^{-1} \quad (21)$$

Degradation Pathways of IBP and NPX in the UV/NH_2Cl AOP. Based on the products identified by UPLC-Q-TOF-MS, the detailed information (i.e., elemental formula and structure) for the products obtained during the degradation of IBP and NPX by the UV/NH_2Cl treatment is provided in Tables S3 and S4. The total ion chromatograms of IBP and NPX are shown in Figures S10 and S12, respectively, and the MS and MS^2 spectra of the IBP and NPX main products are shown in Figures S11 and S13, respectively. Quantum chemistry calculations were used to predict the reaction sites of IBP and NPX. The HOMO molecular orbitals were calculated for IBP and NPX (Figure S14). The HOMO orbitals of both IBP and NPX were dominated by the C atoms on the aromatic rings. This suggested that the attacking sites of IBP and NPX by the radicals are primarily located on aromatic rings. For the side chains of IBP and NPX, C_{11} and C_{24} of IBP (IBP-C_{11}, IBP-C_{24}), O_{17}, and C_{22} of NPX (NPX-O_{17}, NPX-C_{22}) also contributed to the HOMO orbitals. Thus, the reactions of IBP and NPX with radicals can also occur on these

DOI: 10.1021/acs.est.9b01212
Environ. Sci. Technol. 2019, 53, 11142−11152

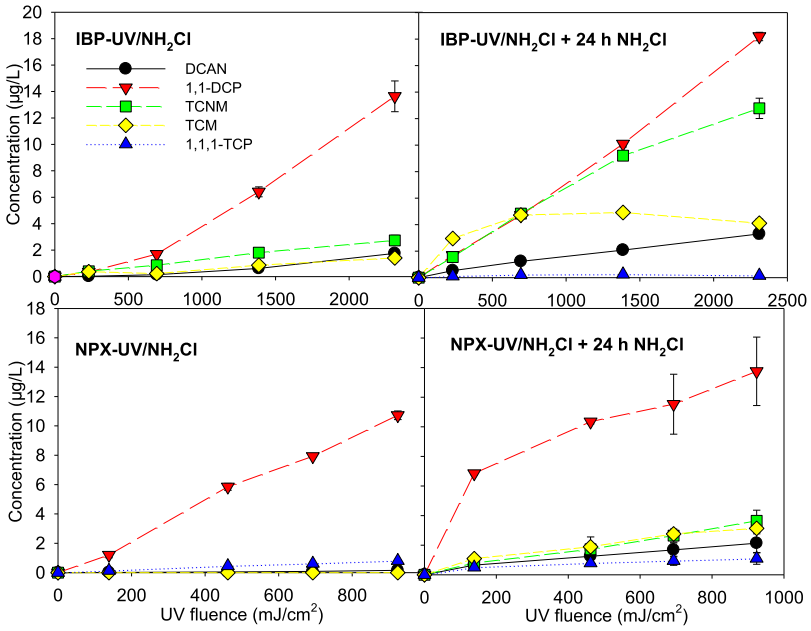

Figure 5. Formation of DBPs during the degradation of IBP and NPX by the UV/NH_2Cl AOP and that followed with post 24 h chloramination. Conditions: $[NH_2Cl]_0$ = 500 μM, $[IBP]_0$ = $[NPX]_0$ = 50 μM, pH = 7.

atoms. Additionally, the partial charges assigned to each atom for the IBP and NPX molecules were calculated and are shown in Table S5. Based on HOMO orbitals and partial charges, IBP-C_5 and NPX-C_{10} located on the aromatic rings provide the main contribution to the HOMO orbitals and have substantial negative charges. Then, the attacking sites by the radicals are located primarily on IBP-C_5 and NPX-C_{10}, respectively. Based on the quantum chemistry calculations, the reaction sites by radicals can be more specific; thus, the structures of the products can be refined.

Figures S15 and S16 show the time-dependent evolution profiles of the major products of IBP and NPX, respectively, during the UV/NH_2Cl AOP at pH 7. During the degradation of IBP, the major products were found at m/z 221[b] ($C_{13}H_{18}O_3$), m/z 283 ($C_{12}H_{16}N_2O_6$), m/z 266[a] ($C_{13}H_{17}NO_5$), and m/z 238[b,d] ($C_{12}H_{17}NO_4$). The abundance of m/z 221[b] initially increased rapidly within 5 min and then decreased (Figure S15), indicating that m/z 221[b] was the initial product generated by IBP degradation. m/z 272[b,c], 300[a,b], and 283[b] were identified as the intermediates because their abundances peaked at 30 min and then decreased. Other products that monotonically increased with reaction time were regarded as the final products or the intermediates with a higher formation rate compared to the degradation rate. For NPX, the predominant products were m/z 201[b] ($C_{13}H_{14}O_2$), m/z 233 ($C_{13}H_{14}O_4$), m/z 290[a] ($C_{14}H_{13}NO_6$), m/z 217[a] ($C_{13}H_{14}O_3$), m/z 218 ($C_{11}H_9NO_4$), m/z 232 ($C_{12}H_{11}NO_4$), m/z 262 ($C_{13}H_{13}NO_5$), and m/z 260[b] ($C_{13}H_{11}NO_5$). Based on the evolution of products' abundance, m/z 201[b] and 290[a] were considered to be the primary products; m/z 217, 280, and 262 were identified as intermediates; and m/z 233 and 260 were regarded as the final products (Figure S16).

Based on the identified intermediates and products, the degradation pathways of IBP and NPX by the UV/NH_2Cl AOP are proposed in Figure 4a,b, respectively. Hydroxylation, demethylation, nitrosation, decarboxylation, and chlorine substitution were the predominant transformation pathways of IBP and NPX by the UV/NH_2Cl AOP. Interestingly, the yields of the nitrogen-containing products were significant compared to the yields of other products during the degradation of IBP and NPX by UV/NH_2Cl, and most of the nitrogen-containing products contained the nitroso-group, indicating that $^{\bullet}NO$ played an important role in the degradation of IBP and NPX by the UV/NH_2Cl AOP. Note that the hydroxylated compounds were the dominant products during IBP and NPX degradation by UV/NH_2Cl in the absence of O_2, and the yields of nitrogen-containing products were relatively low (Table S6 and Figure S17).

In the degradation of IBP, hydroxylation and demethylation were the initial pathways for generating m/z 221[b] and m/z 191[b], respectively. Then, nitrosation and hydroxylation of m/z 221[b] and m/z 191[b] formed m/z 266 and m/z 236[b], respectively. m/z 221[b] was decarboxylated and then produced a series of nitrosation and hydroxylation products such as m/z 238[b,d] and 283[a,b] through a further oxidation by $^{\bullet}NO$ and $HO^{\bullet}$. Chlorine substitution of m/z 266 formed m/z 300[b] through $Cl^{\bullet}$ addition. Then, m/z 300[b] was decarboxylated and oxidized by $HO^{\bullet}$ to form m/z 272[c]. The corresponding abundances of m/z 300[b] and its isotopic peak (M + 2, m/z 302[b]) were 3:1, and those of m/z 272[b,c] and its isotopic peak (M + 2, m/z 274[b,c]) were also 3:1, suggesting that m/z 300 and 272 were monochloro compounds (Figure S11).

In the degradation of NPX, the initial steps included hydroxylation, demethylation, nitrosation, decarboxylation, and chlorine substitution. Hydroxylation and nitrosation generated m/z 290[a], whereas hydroxylation, nitrosation, and demethylation generated m/z 260[b]. Meanwhile, chlorine substitution and demethylation of NPX formed m/z 249, which generated m/z 209 through further oxidation by $HO^{\bullet}$ and cleavage of the side chain. The abundance ratios of m/z 249 to m/z 251 (retention time = 5.32 min) and m/z 209 to m/z 211 (retention time = 3.39 min) were 3:1, suggesting that m/z 249 and 209 were monochloro products (Figure S13). Decarboxylation followed by hydroxylation of NPX formed the mono-, di-, and tri-hydroxylated products of m/z 201[a,b], 217[a,b], and 233[a,b], respectively. Then, hydroxylation, nitrosation, and/

DOI: 10.1021/acs.est.9b01212
Environ. Sci. Technol. 2019, 53, 11142−11152

or demethylation of m/z 201[b] and 217[a] produced m/z 232 and 262, respectively. The cleavage of the side chains of m/z 290[a] and 201[b] was observed to form m/z 218. In addition, hydroxylation and amination of m/z 233 was observed to produce m/z 280.

The pathways of hydroxylation, decarboxylation, demethylation, and chlorine substitution were identified in the UV/Cl_2 AOP for the transformation pathways of IBP and NPX.[36,53] These pathways also happened in the UV/NH_2Cl AOP. However, the unique nitrosation products formed in the UV/NH_2Cl AOP indicates that the RNS was important to the transformation of micropollutants by UV/NH_2Cl.

DBP Formation from IBP and NPX during UV/NH_2Cl and Subsequent Chloramination. Figure 5 shows the formation of DBPs during IBP and NPX degradation during UV/NH_2Cl and that was followed by dark chloramination for 24 h. Five chlorinated DBPs of TCM, 1,1-DCP, 1,1,1-TCP, TCNM, and DCAN were detected during the degradation of both IBP and NPX by UV/NH_2Cl. In the degradation of IBP, 1,1-DCP and TCNM were the major DBPs for which the concentrations reached 13.6 and 2.74 μg/L, respectively, during the UV/NH_2Cl AOP, and these concentrations increased to 18.2 and 12.8 μg/L, respectively, after dark chloramination for 24 h. For NPX, the formation of DBPs was lower than that of IBP. 1,1-DCP was the major DBP, whose concentration reached 10.7 and 13.7 μg/L after 20 min of UV/NH_2Cl treatment and post chloramination, respectively. Interestingly, the TCNM concentration reached 3.64 μg/L after a 20 min UV/NH_2Cl treatment followed by post chloramination for 24 h, but TCNM was not detected during the UV/NH_2Cl treatment. Note that the formation of DBPs during 24 h dark chloramination alone and after UV treatment with post 24 h chloramination was not significant (Figure S18).

For both IBP and NPX, DBP formation increased with increasing UV/NH_2Cl treatment time during UV/NH_2Cl and in post chloramination. This indicates that DBPs were likely to form by the attack of the radicals such as $Cl^\bullet$ and RNS during the UV/NH_2Cl treatment, and additionally, more precursors could be formed by the UV/NH_2Cl treatment to increase the DBP formation in post chloramination. Notably, the high concentration of TCNM further indicates the important roles of RNS in the UV/NH_2Cl AOP that can be carried out by the simultaneous attack of RNS, RCS, and NH_2Cl. Additionally, the precursors containing the nitro-group c6an be formed by further oxidation of products containing the nitroso-group,[54] leading to the formation of TCNM in post chloramination.

Engineering Implication. The UV/NH_2Cl AOP was demonstrated to be an effective AOP for the abatement of micropollutants, and the obtained efficiencies were comparable to that of the UV/Cl_2 AOP. The UV/NH_2Cl AOP was slightly affected by pH, making it effective at a wider pH range. At neutral and alkaline pH, the removal rate of some micropollutants by UV/NH_2Cl was higher than that by UV/Cl_2.[15]

This study first found that RNS especially $^\bullet NO$ played important roles in the UV/NH_2Cl AOP, generating more nitroso-group-containing products and TCNM (a toxic N-DBP) during micropollutants degradation. The production of $^\bullet NO$ in UV/NH_2Cl was proved by EPR, and the roles of $^\bullet NO$ in the degradation kinetics and pathways of micropollutants by the UV/NH_2Cl AOP were significant. The contribution of RNS was significant to the formation of nitro- and nitroso-products during the micropollutants degradation by the UV/NH_2Cl AOP. More importantly, the toxicity induced by RNS after UV/NH_2Cl treatment should be further evaluated because the nitro- and nitroso-group-containing compounds are expected to be more toxic.[55,56] Thus, the involvement of RNS in UV/NH_2Cl should be further evaluated considering the toxicity alternation in real water treatment.

■ ASSOCIATED CONTENT

Supporting Information

The Supporting Information is available free of charge on the ACS Publications website at DOI: 10.1021/acs.est.9b01212.

Pretreatment procedures for sample analyses; chromatographic and mass conditions of UPLC-Q-TOF-MS analysis; determination of the second-order rate constants for $Cl^\bullet$ and steady-state concentrations of $HO^\bullet$, $Cl^\bullet$, and $ClO^\bullet$; characteristics of selected micropollutants; reactive species kinetic model; degradation products of IBP and NPX; partial charges assigned to each atom for IBP and NPX molecular by density functional theory; degradation products of IBP and NPX; photolysis of dilute H_2O_2; formation of nitrite and nitrate in the UV/NH_2Cl system; concentrations of $HO^\bullet$ and $Cl^\bullet$ by experiments and those of $HO^\bullet$, $Cl^\bullet$, $Cl_2^{\bullet-}$, $^\bullet NO$, and $^\bullet NO_2$ by modeling; decay kinetics of NH_2Cl; UV fluence-based pseudo-first order rate constants (k') of IBP and NPX and the specific k' by UV, $HO^\bullet$, $Cl^\bullet$, and other radicals; effect of the radical scavenger t-butanol on the degradation of IBP and NPX; degradation of radical probes of NB, BA, and DMOB; determination of the second-order rate constants for $HO^\bullet$ and $Cl^\bullet$ reacting with IBP and NPX; total ion chromatogram of IBP and NPX; MS and MS^2 spectra of the main products of IBP and NPX; molecular geometries of IBP and NPX and geometries of HOMO molecular orbital for IBP and NPX; time-dependent evolution of major products of IBP and NPX; relative production of transformation products during IBP and NPX degradation; and formation of DBPs during IBP and NPX degradation (PDF)

■ AUTHOR INFORMATION

Corresponding Author

*E-mail: fangjy3@mail.sysu.edu.cn. Phone: +86-18680581522.

ORCID

Zihao Wu: 0000-0002-2407-4448
Ben-Zhan Zhu: 0000-0001-5484-4290
Taicheng An: 0000-0001-6918-8070
Fangang Meng: 0000-0002-7976-9722
Jingyun Fang: 0000-0001-5997-0384

Author Contributions

‖Shared first authorship.

Notes

The authors declare no competing financial interest.

■ ACKNOWLEDGMENTS

This work was financially supported by the Natural Science Foundation of China (21677181, 51908564), the China Postdoctoral Science Foundation (2019M653178), and the Research Fund Program of Guangdong Key Laboratory of Environmental Catalysis and Health Risk Control

DOI: 10.1021/acs.est.9b01212
Environ. Sci. Technol. 2019, 53, 11142−11152

(GKECHRC-01). Finally, we would like to acknowledge Tian Lu for Gaussian09 software support.

REFERENCES

(1) Kong, X.; Wu, Z.; Ren, Z.; Guo, K.; Hou, S.; Hua, Z.; Li, X.; Fang, J. Degradation of lipid regulators by the UV/chlorine process: Radical mechanisms, chlorine oxide radical ($ClO^{\bullet}$)-mediated transformation pathways and toxicity changes. *Water Res.* **2018**, *137*, 242−250.

(2) Pan, Y.; Cheng, S.; Yang, X.; Ren, J.; Fang, J.; Shang, C.; Song, W.; Lian, L.; Zhang, X. UV/chlorine treatment of carbamazepine: Transformation products and their formation kinetics. *Water Res.* **2017**, *116*, 254−265.

(3) Guo, K.; Wu, Z.; Shang, C.; Yao, B.; Hou, S.; Yang, X.; Song, W.; Fang, J. Radical chemistry and structural relationships of PPCP degradation by UV/chlorine treatment in simulated drinking water. *Environ. Sci. Technol.* **2017**, *51*, 10431−10439.

(4) Wu, Z.; Guo, K.; Fang, J.; Yang, X.; Xiao, H.; Hou, S.; Kong, X.; Shang, C.; Yang, X.; Meng, F.; Chen, L. Factors affecting the roles of reactive species in the degradation of micropollutants by the UV/chlorine process. *Water Res.* **2017**, *126*, 351−360.

(5) Qin, L.; Lin, Y.-L.; Xu, B.; Hu, C.-Y.; Tian, F.-X.; Zhang, T.-Y.; Zhu, W.-Q.; Huang, H.; Gao, N.-Y. Kinetic models and pathways of ronidazole degradation by chlorination, UV irradiation and UV/chlorine processes. *Water Res.* **2014**, *65*, 271−281.

(6) Rott, E.; Kuch, B.; Lange, C.; Richter, P.; Minke, R. Influence of ammonium ions, organic load and flow rate on the UV/chlorine AOP applied to effluent of a wastewater treatment plant at pilot scale. *Int. J. Environ. Res. Public Health* **2018**, *15*, 1276.

(7) Chuang, Y.-H.; Szczuka, A.; Shabani, F.; Munoz, J.; Aflaki, R.; Hammond, S. D.; Mitch, W. A. Pilot-scale comparison of microfiltration/reverse osmosis and ozone/biological activated carbon with UV/hydrogen peroxide or UV/free chlorine AOP treatment for controlling disinfection byproducts during wastewater reuse. *Water Res.* **2019**, *152*, 215−225.

(8) Patton, S.; Li, W.; Couch, K. D.; Mezyk, S. P.; Ishida, K. P.; Liu, H. Impact of the ultraviolet photolysis of monochloramine on 1,4-dioxane removal: new insights into potable water reuse. *Environ. Sci. Technol. Lett.* **2017**, *4*, 26−30.

(9) Xu, P.; Bellona, C.; Drewes, J. E. Fouling of nanofiltration and reverse osmosis membranes during municipal wastewater reclamation: Membrane autopsy results from pilot-scale investigations. *J. Membr. Sci.* **2010**, *353*, 111−121.

(10) Soltermann, F.; Widler, T.; Canonica, S.; von Gunten, U. Photolysis of inorganic chloramines and efficiency of trichloramine abatement by UV treatment of swimming pool water. *Water Res.* **2014**, *56*, 280−291.

(11) Weng, S.; Li, J.; Blatchley, E. R. Effects of UV_{254} irradiation on residual chlorine and DBPs in chlorination of model organic-N precursors in swimming pools. *Water Res.* **2012**, *46*, 2674−2682.

(12) Li, J.; Blatchley, E. R., III UV photodegradation of inorganic chloramines. *Environ. Sci. Technol.* **2009**, *43*, 60−65.

(13) Soltermann, F.; Lee, M.; Canonica, S.; von Gunten, U. Enhanced N-nitrosamine formation in pool water by UV irradiation of chlorinated secondary amines in the presence of monochloramine. *Water Res.* **2013**, *47*, 79−90.

(14) Grebel, J. E.; Pignatello, J. J.; Mitch, W. A. Effect of halide ions and carbonates on organic contaminant degradation by hydroxyl radical-based advanced oxidation processes in saline waters. *Environ. Sci. Technol.* **2010**, *44*, 6822−6828.

(15) Chuang, Y.-H.; Chen, S.; Chinn, C. J.; Mitch, W. A. Comparing the UV/monochloramine and UV/free chlorine advanced oxidation processes (AOPs) to the UV/hydrogen peroxide AOP under scenarios relevant to potable reuse. *Environ. Sci. Technol.* **2017**, *51*, 13859−13868.

(16) Zhang, R.; Meng, T.; Huang, C.-H.; Ben, W.; Yao, H.; Liu, R.; Sun, P. PPCP degradation by chlorine−UV processes in ammoniacal water: New reaction insights, kinetic modeling, and DBP formation. *Environ. Sci. Technol.* **2018**, *52*, 7833−7841.

(17) Patton, S.; Romano, M.; Naddeo, V.; Ishida, K. P.; Liu, H. Photolysis of mono- and dichloramines in UV/hydrogen peroxide: effects on 1,4-dioxane removal and relevance in water reuse. *Environ. Sci. Technol.* **2018**, *52*, 11720−11727.

(18) Li, W.; Patton, S.; Gleason, J. M.; Mezyk, S. P.; Ishida, K. P.; Liu, H. UV photolysis of chloramine and persulfate for 1,4-dioxane removal in reverse-osmosis permeate for potable water reuse. *Environ. Sci. Technol.* **2018**, *52*, 6417−6425.

(19) Zhang, X.; Li, W.; Blatchley, E. R.; Wang, X.; Ren, P. UV/chlorine process for ammonia removal and disinfection by-product reduction: Comparison with chlorination. *Water Res.* **2015**, *68*, 804−811.

(20) Goldstein, S.; Rabani, J. Mechanism of nitrite formation by nitrate photolysis in aqueous solutions: The role of peroxynitrite, nitrogen dioxide, and hydroxyl radical. *J. Am. Chem. Soc.* **2007**, *129*, 10597−10601.

(21) Yang, P.; Ji, Y.; Lu, J.; Huang, Q. Formation of nitrophenolic byproducts during heat-activated peroxydisulfate oxidation in the presence of natural organic matter and nitrite. *Environ. Sci. Technol.* **2019**, *53*, 4255−4264.

(22) NIST. The Radiation Chemistry Data Center of the Notre Dame Radiation Laboratory (ndrlRCDC) Kinetics Database. kinetics.nist.gov/solution/SearchForm, 2019 (accessed Jan 10, 2019).

(23) Liu, Y.; Wang, Q.; Pan, J. Novel process on simultaneous removal of nitric oxide and sulfur dioxide using vacuum ultraviolet (VUV)-activated $O_2/H_2O/H_2O_2$ system in a wet VUV-spraying reactor. *Environ. Sci. Technol.* **2016**, *50*, 12966.

(24) Yang, L.; Schoenfisch, M. H. Nitric oxide-releasing hyperbranched polyaminoglycosides for antibacterial therapy. *ACS Appl. Bio Mater.* **2018**, *1*, 1066−1073.

(25) Huang, Y.; Kong, M.; Westerman, D.; Xu, E. G.; Coffin, S.; Cochran, K. H.; Liu, Y.; Richardson, S. D.; Schlenk, D.; Dionysiou, D. D. Effects of HCO_3^- on degradation of toxic contaminants of emerging concern by UV/NO_3^-. *Environ. Sci. Technol.* **2018**, *52*, 12697−12707.

(26) Scholes, R. C.; Prasse, C.; Sedlak, D. L. The role of reactive nitrogen species in sensitized photolysis of wastewater-derived trace organic contaminants. *Environ. Sci. Technol.* **2019**, *53*, 6483−6491.

(27) Kong, X.; Jiang, J.; Ma, J.; Yang, Y.; Liu, W.; Liu, Y. Degradation of atrazine by UV/chlorine: Efficiency, influencing factors, and products. *Water Res.* **2016**, *90*, 15−23.

(28) Wu, Z.; Fang, J.; Xiang, Y.; Shang, C.; Li, X.; Meng, F.; Yang, X. Roles of reactive chlorine species in trimethoprim degradation in the UV/chlorine process: Kinetics and transformation pathways. *Water Res.* **2016**, *104*, 272−282.

(29) Goldstein, S.; Johan, L.; Gábor, M. Chemistry of peroxynitrites as compared to peroxynitrates. *Chem. Rev.* **2005**, *105*, 2457−2470.

(30) Quintana, J. B.; Rodil, R.; Rodríguez, I. *Transformation Products of Emerging Contaminants in the Environment: Analysis, Processes, Occurrence, Effects and Risks*; Wiley, 2014.

(31) Lyon, B. A.; Dotson, A. D.; Linden, K. G.; Weinberg, H. S. The effect of inorganic precursors on disinfection byproduct formation during UV-chlorine/chloramine drinking water treatment. *Water Res.* **2012**, *46*, 4653−4664.

(32) Hand, V. C.; Margerum, D. W. Kinetics and mechanisms of the decomposition of dichloramine in aqueous solution. *Inorg. Chem.* **1983**, *22*, 1449−1456.

(33) Bolton, J. R.; Linden, K. G. Standardization of methods for fluence (UV dose) determination in bench-scale UV experiments. *J. Environ. Eng.* **2003**, *129*, 209−215.

(34) Garoma, T.; Gurol, M. D. Modeling aqueous ozone/UV process using oxalic acid as probe chemical. *Environ. Sci. Technol.* **2005**, *39*, 7964−7969.

(35) Michael, I.; Hapeshi, E.; Osorio, V.; Perez, S.; Petrovic, M.; Zapata, A.; Malato, S.; Barceló, D.; Fatta-Kassinos, D. Solar photocatalytic treatment of trimethoprim in four environmental matrices at a pilot scale: transformation products and ecotoxicity evaluation. *Sci. Total Environ.* **2012**, *430*, 167−173.

DOI: 10.1021/acs.est.9b01212
Environ. Sci. Technol. 2019, 53, 11142−11152

(36) Pan, M.; Wu, Z.; Tang, C.; Guo, K.; Cao, Y.; Fang, J. Emerging investigators series: comparative study of naproxen degradation by the UV/chlorine and the UV/H_2O_2 advanced oxidation processes. *Environ. Sci.: Water Res. Technol.* **2018**, *4*, 1219−1230.
(37) Hua, Z.; Guo, K.; Kong, X.; Lin, S.; Wu, Z.; Wang, L.; Huang, H.; Fang, J. PPCP degradation and DBP formation in the solar/free chlorine system: Effects of pH and dissolved oxygen. *Water Res.* **2019**, *150*, 77−85.
(38) USEPA. *Standard Methods for the Examination of Water and Wastewater*, 22nd ed.; American Public Health Assoc: Washington, DC, USA, 2012.
(39) Alegre, M. L.; Geronés, M.; Rosso, J. A.; Bertolotti, S. G.; Braun, A. M.; Mártire, D. O.; Gonzalez, M. C. Kinetic study of the reactions of chlorine atoms and $Cl_2^{\bullet-}$ radical anions in aqueous solutions. 1. Reaction with benzene. *J. Phys. Chem. A* **2000**, *104*, 3117−3125.
(40) Cao, Y. L.; Guo, P.; Xu, Y. C.; Zhao, B. L. Simultaneous detection of NO and ROS by ESR in biological systems. In *Methods in Enzymology*; Packer, L., Cadenas, E., Eds.; Elsevier, 2005; Vol. *396*, pp 77−83.
(41) Zhu, B.-Z.; Zhao, H.-T.; Kalyanaraman, B.; Frei, B. Metal-independent production of hydroxyl radicals by halogenated quinones and hydrogen peroxide: An ESR spin trapping study. *Free Radic. Biol. Med.* **2002**, *32*, 465−473.
(42) Chen, L.; Li, X.; Zhang, J.; Fang, J.; Huang, Y.; Wang, P.; Ma, J. Production of hydroxyl radical via the activation of hydrogen peroxide by hydroxylamine. *Environ. Sci. Technol.* **2015**, *49*, 10373−10379.
(43) USEPA. *Standard Methods for the Examination of Water and Wastewater*, 20th ed.; American Public Health Assoc: Washington, DC, USA, 1998.
(44) Frisch, G. W. T. M.; Schlegel, H. B.; Scuseria, G. E.; Robb, M. A.; Cheeseman, J. R.; Scalmani, G.; Barone, V.; Mennucci, B.; Petersson, G. A.; Nakatsuji, H.; Caricato, M.; Li, X.; Hratchian, H. P.; Izmaylov, A. F.; Bloino, J.; Zheng, G.; Sonnenberg, J. L.; Hada, M.; Ehara, M.; Toyota, K.; Fukuda, R.; Hasegawa, J.; Ishida, M.; Nakajima, T.; Honda, Y.; Kitao, O.; Nakai, H.; Vreven, T.; Montgomery, J. A., Jr.; Peralta, J. E.; Ogliaro, F.; Bearpark, M.; Heyd, J. J.; Brothers, E.; Kudin, K. N.; Staroverov, V. N.; Keith, T.; Kobayashi, R.; Normand, J.; Raghavachari, K.; Rendell, A.; Burant, J. C.; Iyengar, S. S.; Tomasi, J.; Cossi, M.; Rega, N.; Millam, J. M.; Klene, M.; Knox, J. E.; Cross, J. B.; Bakken, V.; Adamo, C.; Jaramillo, J.; Gomperts, R.; Stratmann, R. E.; Yazyev, O.; Austin, A. J.; Cammi, R.; Pomelli, C.; Ochterski, J. W.; Martin, R. L.; Morokuma, K.; Zakrzewski, V. G.; Voth, G. A.; Salvador, P.; Dannenberg, J. J.; Dapprich, S.; Daniels, A. D.; Farkas, Ö.; Foresman, J. B.; Ortiz, J. V.; Cioslowski, J.; Fox, D. J. *Gaussian*, Gaussian 09, revision C.01; Gaussian, Inc.: Wallingford CT, 2010.
(45) Ianni, J. C. *Kintecus*, Windows version 5.50, 2018.
(46) De Laat, J.; Boudiaf, N.; Dossier-Berne, F. Effect of dissolved oxygen on the photodecomposition of monochloramine and dichloramine in aqueous solution by UV irradiation at 253.7 nm. *Water Res.* **2010**, *44*, 3261−3269.
(47) Margerum, D. W.; Schurter, L. M.; Hobson, J.; Moore, E. E. Water chlorination chemistry: Nonmetal redox kinetics of chloramine and nitrite ion. *Environ. Sci. Technol.* **1994**, *28*, 331−337.
(48) Laszlo, B.; Alfassi, Z. B.; Neta, P.; Huie, R. E. Kinetics and mechanism of the reaction of $^{\bullet}NH_2$ with O_2 in aqueous solutions. *J. Phys. Chem. A* **1998**, *102*, 8498−8504.
(49) Finkelstein, E.; Rosen, G. M.; Rauckman, E. J. Spin trapping. Kinetics of the reaction of superoxide and hydroxyl radicals with nitrones. *J. Am. Chem. Soc.* **1980**, *102*, 4994−4999.
(50) Zhang, Z.; Chuang, Y.-H.; Huang, N.; Mitch, W. A. Predicting the contribution of chloramines to contaminant decay during ultraviolet/hydrogen peroxide advanced oxidation process treatment for potable reuse. *Environ. Sci. Technol.* **2019**, *53*, 4416−4425.
(51) Hasegawa, K.; Neta, P. Rate constants and mechanisms of reaction of chloride (Cl_2^-) radicals. *J. Phys. Chem.* **1978**, *82*, 854−857.
(52) Fang, J.; Fu, Y.; Shang, C. The roles of reactive species in micropollutant degradation in the UV/free chlorine system. *Environ. Sci. Technol.* **2014**, *48*, 1859−1868.
(53) Xiang, Y.; Fang, J.; Shang, C. Kinetics and pathways of ibuprofen degradation by the UV/chlorine advanced oxidation process. *Water Res.* **2016**, *90*, 301−308.
(54) Vione, D.; Maurino, V.; Minero, C.; Pelizzetti, E. Phenol photonitration upon UV irradiation of nitrite in aqueous solution I: Effects of oxygen and 2-propanol. *Chemosphere* **2001**, *45*, 893−902.
(55) Shah, A. D.; Mitch, W. A. Halonitroalkanes, halonitriles, haloamides, and N-nitrosamines: a critical review of nitrogenous disinfection byproduct formation pathways. *Environ. Sci. Technol.* **2012**, *46*, 119.
(56) Wang, L.-S.; Hong-Ying, H.; Chao, W. Effect of ammonia nitrogen and dissolved organic matter fractions on the genotoxicity of wastewater effluent during chlorine disinfection. *Environ. Sci. Technol.* **2007**, *41*, 160−165.

DOI: 10.1021/acs.est.9b01212
Environ. Sci. Technol. 2019, 53, 11142−11152